

BRNO UNIVERSITY OF TECHNOLOGY
VYSOKÉ UČENÍ TECHNICKÉ V BRNĚ

**FACULTY OF ELECTRICAL ENGINEERING AND
COMMUNICATION**
FAKULTA ELEKTROTECHNIKY A KOMUNIKAČNÍCH TECHNOLOGIÍ

DEPARMENT OF RADIO ELECTRONICS
ÚSTAV RADIOELEKTRONIKY

TEXTILE INTEGRATED WAVEGUIDE COMPONENTS
KOMPONENTY NA BÁZI VLNOVODU INTEGROVANÉHO DO TEXTILU

SHORTED VERSION OF DOCTORAL THESIS

Author (Autor práce)
Ing. Miroslav Cupal

Supervisor (Školitel)
Prof. Dr. Ing. Zbyněk Raida

Defense date (Datum obhajoby)
22. 4. 2020

Opponents (Oponenti)

KEYWORDS

Textile integrated waveguide (TIW), 3D knitted fabric, conductive yarn, screen-printing, conductive adhesive, circularly polarized antenna, reconfigurable switch, transition from conventional to textile-integrated line.

KLÍČOVÁ SLOVA

Vlnovod integrovaný do textilu (TIW), 3D tkaná textilie, vodivá nit, sítotisk, vodivé lepidlo, kruhově polarizovaná anténa, rekonfigurovatelný přepínač, přechod z konvenčního vedení na vedení integrované do textilu.

STORAGE PLACE

Research department, FEEC BUT, Technická 3058/10, 602 00 Brno

MÍSTO ULOŽENÍ PRÁCE

Vědecké oddělení, FEKT VUT v Brně, Technická 3058/10, 602 00 Brno

© Miroslav Cupal 2020

ISBN (80-214-)

ISSN 1213-4198

Contents

INTRODUCTION.....	4
1 STATE OF THE ART.....	5
1.1 Textile-integrated high-frequency antennas.....	5
1.2 Textile-integrated switches	6
1.3 Textile-to-conventional line transitions	7
1.4 Conclusions	7
2 OBJECTIVES	8
3 TEXTILE TO CONVENTIONAL LINE TRANSITIONS.....	9
3.1 Design of MTL-to-TIW transition	9
3.1 Results of SIMULATION AND measurements	11
3.4 Conclusions	12
4 TEXTILE INTEGRATED SWITCH.....	13
4.1 Switch design and simulations	13
4.2 Switch manufacturing and measurements.....	14
4.3 Conclusions	15
5 CYRCULARLY POLARIZED TEXTILE-INTEGRATED ANTENNAS	17
5.1 Design of textile-integrated antennas.....	17
5.2 Simulation, implementation and measurement of TIW antennas	20
5.3 Conclusions.....	25
6 TECHNOLOGICAL ASECTS	26
6.1 Conductive threads.....	26
6.2 Measurement of threads and results.....	27
6.3 Conclusions	29
7 SUMMARY	29
8 REFERENCES.....	31
CURRICULUM VITAE	34
ABSTRACT	36

INTRODUCTION

The integration of electronic devices into clothing and textile materials became popular in the late 1990s with the spread of wearable devices and local body area networks. The first textile antennas and other textile components were designed for military, space and healthcare applications. Researchers and companies were focused on the characterization of textile materials, development of conductive textiles, conductive yarns, and complete textile electronic solutions.

The majority of textile-integrated electronics (TIE) can be found in wearable applications. Attention is paid to manufacturing technologies, integration to clothes, biological effects, influence of human body on antenna parameters, launder-ability, abrasion, mechanical stability, etc. Nevertheless, TIE can be also integrated into upholstery in homes, cars, trains or airplanes. The dissertation thesis deals with the non-wearable exploitation of TIE and is dominantly focused on vehicular applications.

The role of the textile substrate is played by the three-dimensional (3D) knitted fabrics. The 3D fabric is used as an equivalent of a conventional microwave substrate. As an equivalent of a substrate-integrated waveguide (SIW), a textile-integrated waveguide (TIW) can be created and can be used as a fundamental building block of textile-integrated structures.

TIW can be integrated into textile covers of seats and textile upholstery of trains, airplanes and buses to create a local communication network. TIW can provide services for passengers or can be used as a backup for control and sensor systems. Each seat in a vehicle can contain a tablet, a sensor network for passenger's personal use and other electronic components to be connected. TIW can create a wired local network within the seat and further communication can be provided by a wireless link. Textile antennas and textile microwave components seem to be a promising way to implement the described local networks.

Next to the wireless interface, attention is turned to the development of textile-to-substrate transitions enabling to create also a wired connection of TIE.

Implementation of TIE can become a part of the manufacturing process of textile materials. Such multi-functional fabrics can be then used not only for attenuating mechanical vibrations, providing thermal insulation and conventional utility properties but also can yield communication and sensory resources. The use of multi-functional textile materials can significantly reduce manufacturing and assembling costs.

The dissertation thesis is mainly aimed to research technologies to be used for the design and implementation of advanced TIW and TIW-based radio-frequency (RF) components. Attention is turned to the development of new components for industrial, scientific and medical (ISM) bands 2.4 GHz, 5.8 GHz and 24 GHz.

1 STATE OF THE ART

Clothing, military applications, space products and healthcare systems belong to the main application areas of textile electronics. A heating layer integrated into clothing was the first exploitation of e-textiles. Conductive fibers were knitted into a conventional textile material and were fed by a current to heat the user [1].

These days, more than 300 000 results can be found when searching for the keyword *textile electronics* in the open literature. Most of textile electronic applications are designed for on-body systems and wearable applications, i.e. sensors for medical and sports systems, communication units for smartphones and other devices, localization and for the emergency services, etc. A brief description of basic textile electronic applications follows.

1.1 TEXTILE-INTEGRATED HIGH-FREQUENCY ANTENNAS

As shown in previous chapters, the majority of papers is focused on manufacturing TIE using different textile materials (polyester, cotton and their combinations) as substrates and different materials for creating conductive layouts. Copper foils are often used for the first prototyping and manufacturing reference structures to be compared with printing technologies.

Textile integrated waveguides (TIW) are a textile version of conventional substrate integrated waveguides (SIW) with some specific properties. Unlike a microstrip line or a coplanar waveguide, TIW is a closed system. TIW can be therefore touched by the human and even bent with a minimal affection to parameters. TIW allows microwave components (antennas and filters) to be coupled with. TIW can be manufactured by all commonly used technologies like printing, plating or embroidering. Nevertheless, embroidering is not suitable for creating more complicated structures containing slots or transitions. Therefore, more complicated TIW antennas are usually manufactured from an electrically conductive textile (ECT), from a copper foil, by screen-printing or inkjet-printing [2, 4, 5]. Manufacturing of top and bottom conductive walls of TIW structures is going to be described in following paragraphs.

In the open literature, three ways of manufacturing sidewalls of TIW were described:

- **Metal eyelets.** Eyelets have a good electrical conductivity and stability. On the other hand, their dimensions are relatively large [6].
- **Conductive yarns.** Relatively high resistivity of yarns is the main disadvantage of sewing sidewalls by yarns. The usual resistivity varies from 10 Ω/m to 100 $\text{k}\Omega/\text{m}$ [7], [8].
- **Electrically conductive textile (ECT).** The textile substrate is cut to form a dielectric filler of the waveguide, and this filler is completely covered by ECT. Unfortunately, manufacturing is rather demanding, and TIW is not integrated into a textile substrate completely.

TIWs, TIW-based components (filters, antennas) and their properties were presented in [6], [8]. The described TIW was designed for the frequency 2.4 GHz using a textile material with $\epsilon_r = 1.45$, $\tan \delta = 0.017$ and thickness $h = 3.94$ mm. The TIW was connected to a SMA connector by a conventional microstrip-to-TIW transition. Sidewalls were created by eyelets and conductive layers by a copper ECT. The average value of transmission coefficient was $S_{21} = -2$ dB.

The substrate integrated folded waveguide (SIFW) is a double-layer version of SIW [6]. The layers inside the waveguide are partly separated by a conductive wall and partly are adjoint. That way, dimensions of the structure can be reduced. As shown in [6], SIFW can be used for the design of a bandpass filter: the operation frequency was 2.4 GHz and the insertion loss at 2.45 GHz was 2.3 dB. Finally, [6] presented a

cavity backed patch antenna designed for the frequency 2.4 GHz with the gain 5.93 dBi and the efficiency 74%. The presented results show that TIW components designed for the ISM band 2.4 GHz can reach reasonable parameters.

In [9], a textile microstrip-fed cavity antenna designed for the ISM band 2.4 GHz was presented. The cavity was created by eyelets, the H-shaped slot was etched in the top conductive layer and the microstrip feeder was placed on the bottom. The free-space gain of the antenna was 3.9 dBi and the efficiency 68%. The front-to-back ratio of the antenna was about 20 dB. Feeding on the bottom is a disadvantage because the microstrip can be affected by surroundings. The described antenna was completed by solar energy-harvesting system; the effect on antenna parameters was presented in [10]. The solar system generated the power from 100 μ W to 400 μ W.

In [8], a TIW for the ISM band 5.8 GHz was presented. The sidewalls were created from a conductive yarn with conductivity 10 Ω /m and TIW was fed by a coaxial probe. The average transmission coefficient S_{21} was -2.3 dB for 135 mm long TIW. The TIW was tested for tension, bending and torsion with a small decrease of S_{21} (about 0.6 dB). A design of a HMTIW antenna was presented in [11]. The sidewalls of the antenna were manufactured by two technologies – using a conductive yarn and a seam compression. In case of seam compression, conductivity of sidewalls was higher, and efficiency of the antenna was better. Nevertheless, the seam compression shifted the resonance frequency of the antenna.

1.2 TEXTILE-INTEGRATED SWITCHES

Textile-integrated switches can be a part of a TIW network to switch among applications, frequency bands or antennas with different radiation patterns. In the open literature, no TIW switches have been described yet. Therefore, an overview of conventional SIW switches is provided.

Depending on the switching method, conventional SIW switches can be divided into three groups:

- **Mechanically driven switch** was designed in [12] for V and W bands. A T-divider was a fundamental building block of the switch with 4 metalized via holes in each arm. These holes were mechanically short-circuited to mirror the electromagnetic (EM) wave. If not short-circuited, the via holes were *invisible* for the EM wave.
- **Magnetically driven switch** based on a ferrite-loaded SIW shifted the cutoff frequency of the L-folded SIW (LFSIW). The shift of the cutoff frequency was considered as switching. The LFSIW is formed by folding a SIW along its longitudinal axis. The LFSIW switch [30] was designed for the frequency 10 GHz and its bandwidth was 1.1 GHz. The isolation was 20 dB and the insertion loss was below 1 dB.
- **Electronically driven switch** with PIN diodes was used for shorting via holes in arms of the SIW divider [13], for shorting slots [14] or for switching between the HMSIW structure and the SIW one [15]. Finally, stubs can be shorted and opened [16].

Since mechanic switches need nonflexible materials and magnetic materials can be hardly integrated into textile materials, attention is paid to electrically driven SIW switches. A switchable T-divider with via holes short-circuited by PIN diodes [13] had 3 via holes in each branch to create a mirror. The insertion loss was lower than 2.5 dB in the open branch and the isolation was higher than 10 dB. The slot on the top layer was used to create an attenuating impedance. Switches based on HMSIW were presented in [15, 16]. In [16], stubs were connected to the virtual wall of the HMSIW and were short-circuited or open-circuited by PIN diodes. If short-circuited, the virtual wall was damaged and the HMSIW had a high attenuation. In [15], a HMSIW was connected with a common SIW wall by PIN diodes. Connecting the second wall to the HMSIW, the cutoff frequency of the structure was changed, and the attenuation became high.

1.3 TEXTILE-TO-CONVENTIONAL LINE TRANSITIONS

As shown in [3], even relatively complicated devices can be printed on textile materials or thin film interposers. But:

- Soldering on textile substrates (with printed electronics, especially) is very complicated.
- Some components (transceivers, e.g.) need an additional shield which is difficult to be manufactured from textile materials.
- Majority of textile antennas, which are designed for personal or local area networks, are expected to be fed by a coaxial cable. But coaxial cables integrated into clothes are impractical from the viewpoint of users.

Therefore, transitions between conventional microwave substrates (Arlon, Rogers, FR4) and textile materials have to be developed.

In the thesis, attention is paid to two-layer transitions between a SIW and a microstrip transmission line (MTL) on a conventional substrate. In [3], advanced electronics was on a conventional substrate, an antenna and a micro-controller unit (MCU) were on a polyethylene terephthalate (PET), interposer, and a transition between a transceiver and an antenna was not solved.

Transitions between MTL on a ceramic substrate and MTL on a textile one were published in [17, 18]. These transitions had a metallic connection between those two MTLs. The first MTL had characteristic impedance $50\ \Omega$ and the second one $75\ \Omega$. In [19,20], a connection by *Snap-On* buttons was investigated and compared with other methods to be used for connecting microstrips. A connection of microstrips on a non-flexible substrate and a flexible one was shown in [21]: the force to keep the connection was given by permanent magnets.

TIWs are usually fed by coaxial cables. According to author's best knowledge, a two-layer transition between TIW and MTL has not been published yet. As demonstrated in [22], a two-layer transition between MTL and SIW can be created with the transmission $S_{21} \approx -1.8\ \text{dB}$ at the frequency 5 GHz.

1.4 CONCLUSIONS

The *State of the Art* results in the following conclusions:

- Basic textile integrated elements, electronic components and sensors are well described in the open literature. Publications comprise various textile materials playing the role of the printed-circuit board (PCB) and different technologies to create electronic components (embroidering, several types of printing). Various structures designed for ISM bands up to 5.8 GHz are presented. In order to investigate frequency limits of textile electronics, an antenna for the ISM band 24 GHz is designed and characterized in the thesis.
- Despite all the efforts, integration of advanced electronics (transceivers, e.g.) to textile materials is difficult and is done impractically by coaxial cables. Therefore, the thesis deal with the transitions between conventional substrates and textile materials.
- TIW structures are very practical because a closed system is created. There are many papers on TIWs and TIW-based antennas but more complicated components like textile-integrated filters, switches or reconfigurable structures have not been described yet. Therefore, the thesis is focused on more complicated textile elements and their configurability. Considering these conclusions, objectives of the dissertation thesis are formulated in the following chapter.

2 OBJECTIVES

The previous part showed the progress in the integration of electronics into textile materials and in techniques of manufacturing textile-integrated microwave components. Many textile antennas for ISM bands 2.4 GHz and 5.8 GHz were presented in the open literature as an isolated part of electronic systems without any connection to the transmitter or receiver. Only a limited number of advanced components (couplers, switches) was described. Considering these facts, three objectives of the dissertation thesis can be formulated.

Objective 1

Design methodology for transitions between MTL on a conventional (non-flexible) substrate and a textile (flexible) substrate will be formulated with emphasis on the transition between two MTLs and between MTL and TIW. The transitions between two MTLs at two frequencies, and the transition between TIW and MTL will be designed and experimentally verified.

Objective 2

Methodology of the integration of advanced and reconfigurable microwave components into textile materials will be formulated. In the thesis, a TIW-based switch with PIN diodes will be described. The switch can be used for switching two antennas with different radiation patterns.

Objective 3

Methodology of the synthesis of a TIW antenna for the ISM band 24 GHz will be formulated. The antenna can be used for future wireless communication systems in public transportation and can be integrated into textile upholstery of vehicles.

3 TEXTILE TO CONVENTIONAL LINE TRANSITIONS

Textile materials can be considered as low-permittivity substrates for frequency range from 0 GHz to 60 GHz [23]. Therefore, dimensions of $50\ \Omega$ transmission lines and antennas are larger compared to conventional microwave substrates (Arlon, Rogers, FR4) of the same thickness. Next, thickness of textile substrates usually ranges from 0.5 mm to 5 mm [1], and the width of the microstrip can be from 2 mm to 15 mm for $50\ \Omega$ MTL [18, 20] when considering a common relative permittivity of the textile. The problem can be solved by microstrips with a higher characteristic impedance (up to $100\ \Omega$) [24]. Nevertheless:

- The width of $100\ \Omega$ MTL on a 3D knitted fabric 3D041 is 5 mm and connecting a transmitter or a receiver is still difficult.
- Transmitters and receivers are designed for $50\ \Omega$ impedances. The use of $100\ \Omega$ transmission lines leads to mismatch and additional losses.

3.1 DESIGN OF MTL-TO-TIW TRANSITION

A two-layer transition between TIW and MTL on a conventional substrate is based on a current probe which is used for feeding waveguides or SIWs. This transition can connect electronics on a conventional substrate and textile-integrated antennas. Antennas can be designed on a textile substrate without difficulties. Some subsystems like RF circuits are too small and sensitive for manufacturing precision and have to be designed on a conventional PCB. The transition allows to connect TIW working with the dominant TE_{10} mode and MTL with a different characteristic impedance on a conventional substrate. The mechanical connection between TIW and PCB is given by a metal wire used as a current probe. Moreover, the connection can be supported by additional mechanic supports. Hence, a strong connection protected against mechanical damage can be created.

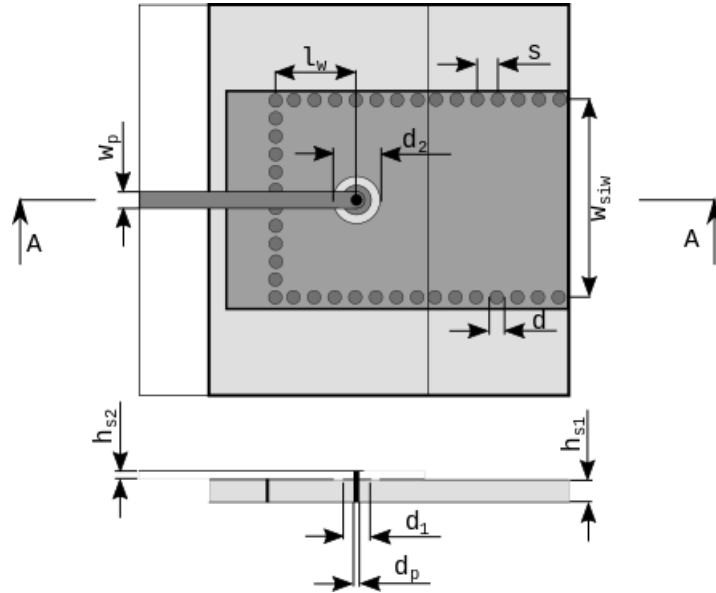


Figure 1 MTL-to-TIW transition with dimensions.

The distance between the short-circuited termination of TIW and the shorting pin l_{dp1} is an important parameter. The proper distance has to be $\lambda_g/4$ where λ_g is the wavelength in TIW (the pin is in the maximum of electric field). On the top side of TIW and on the ground side of MTL, a circular slot is created. The slot

is centered around the shorting pin and its diameter can be calculated as the diameter of a corresponding coaxial cable [25]. The bandwidth of the transition can be increased by a circular ring around the shorting pin which compensates its inductance [26].

Transitions were designed for the textile substrate 3D097 ($\epsilon_{r1} = 1.22$, $\tan \delta_1 = 0.002$, $h_{hs1} = 2.6$ mm) and two different conventional substrates. For the UWB band, we used Arlon 25N ($\epsilon_{r2} = 3.38$, $\tan \delta_2 = 0.0025$, $h_{s2} = 0.762$ mm). For the ISM band, we used FR4 ($\epsilon_{r3} = 4.2$, $\tan \delta_3 = 0.02$, $h_{s3} = 1.52$ mm). The FR4 was chosen because this material is often used for the construction of electronic devices. The design procedure is the same for both the transitions:

- MTL on the conventional substrate is designed;
- TIW with short-circuited termination is designed;
- Wavelength in TIW is calculated, shorting pin is installed in the distance $\lambda_g/4$ from the termination;
- Circular slot around shorting pin is designed (the same impedance as MTL);
- Circular metal ring around shorting pin is designed (initial radius is half of the slot radius).

The designed transition is shown in Figure 1, dimensions of transitions are given in Table 1.

Table 1 Dimensions of MTL-to-TIW transitions for ISM and UWB bands.

dim [mm]	w_{siw}	l_w	d	d_p	d_1	d_2	w_p	h_{s1}	h_{s2}	s
ISM	50	19.1	0.3	1.0	2.0	5.2	2.8	2.6	1.52	2.0
UWB	23	13.2	0.3	2.0	2.0	4.6	1.7	2.6	0.76	2.0
ISM (75 Ω)	50	19.1	0.3	0.4	2.1	4.0	1.3	2.6	1.52	2.0

Attention is turned to outputs of simulations of the ISM 5.8 GHz transition. The top MTL was designed on FR4 and the bottom TIW on the 3D textile 3D097. The transition was simulated with SMA connected to MTL and the waveguide port at the end of TIW. The reflection coefficient was $S_{11} = -24.2$ dB and the transmission $S_{21} = -0.32$ dB. The MTL-to-TIW transition can be designed even for microstrips with the characteristic impedance which differs from 50 Ω . In order to approve the concept, the transition was designed for the microstrip with the characteristic impedance 75 Ω . Performance of the designed transition was verified by simulations (see Figure 2 right). The transition was designed according to rules described in the previous section. Dimensions of the transition are given in Table 1. The reflection coefficient is $S_{11} = -25.47$ dB and the transmission coefficient is $S_{21} = -0.11$ dB.

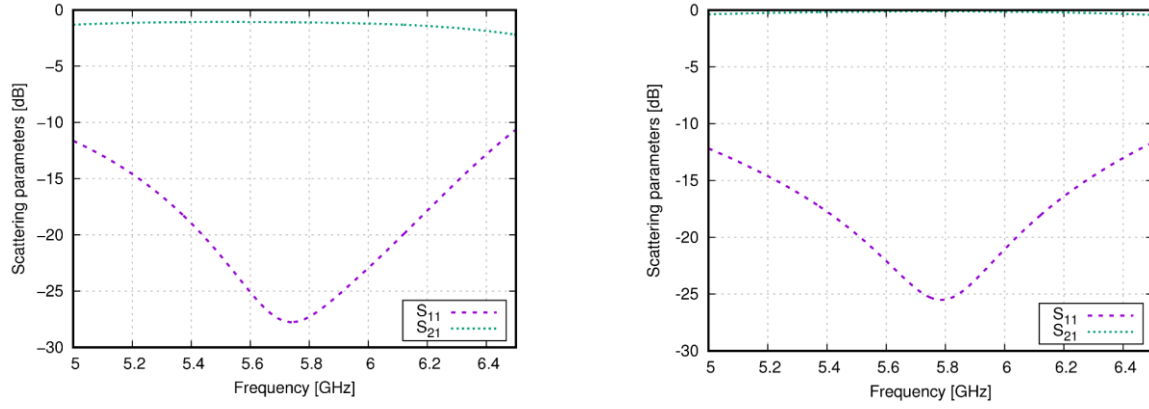


Figure 2 MTL-to-TIW transition for ISM band: simulated reflection and transmission coefficient for 50 Ω microstrip (left) and 75 Ω microstrip (right).

3.1 RESULTS OF SIMULATION AND MEASUREMENTS

For the experimental verification, two transitions operating in the ISM band 5.8 GHz and two transitions operating in the UWB band were manufactured and connected by TIW (see Figure 3). Manufacturing and technological details are provided in Chapter 6.



Figure 3 Photographs of manufactured MTL-to-TIW transitions (ISM left; UWB right).

Results of simulations and measurements of these transitions are shown in Figure 4 and Figure 5. The ISM transition has the simulated insertion loss 2.32 dB (the measured one is 3.12 dB) and the simulated reflection coefficient at the SMA input is $S_{11} = -19.22$ dB (the measured one is -17.23 dB). The maximum of the transmission is shifted to a lower frequency than 5.8 GHz. The minimum of the reflection coefficient is shifted to a frequency lower for about 100 MHz.

The UWB transitions were optimized to maximize the bandwidth where $S_{11} < -10$ dB. The insertion loss varies for less than 3 dB in the band-group 6. Results of measurements show that the reflection coefficient is higher than -10 dB in a lower part of the UWB band and the insertion loss varies from 1.1 dB to 4.3 dB.

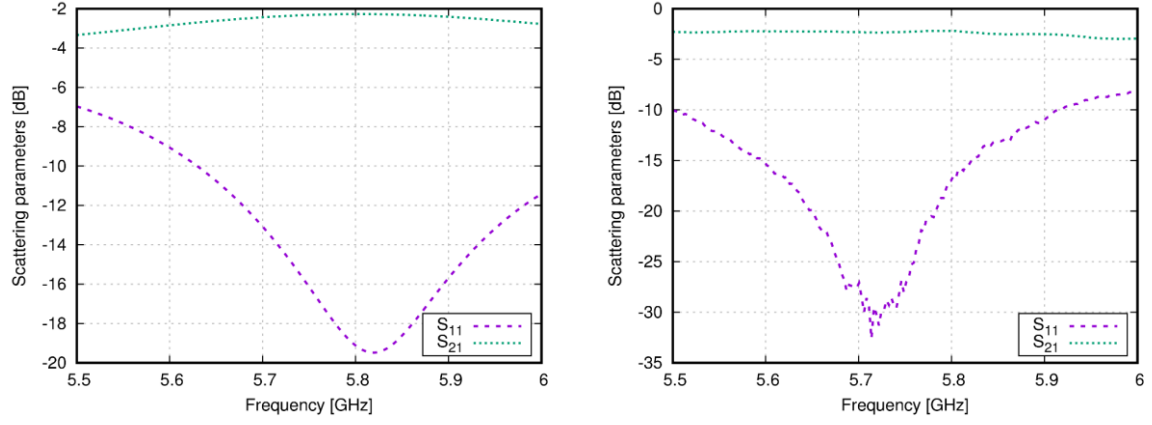


Figure 4 MTL-to-TIW transition for ISM band: simulated S parameters (left) and measured S parameters (right). Configuration from Figure 3.

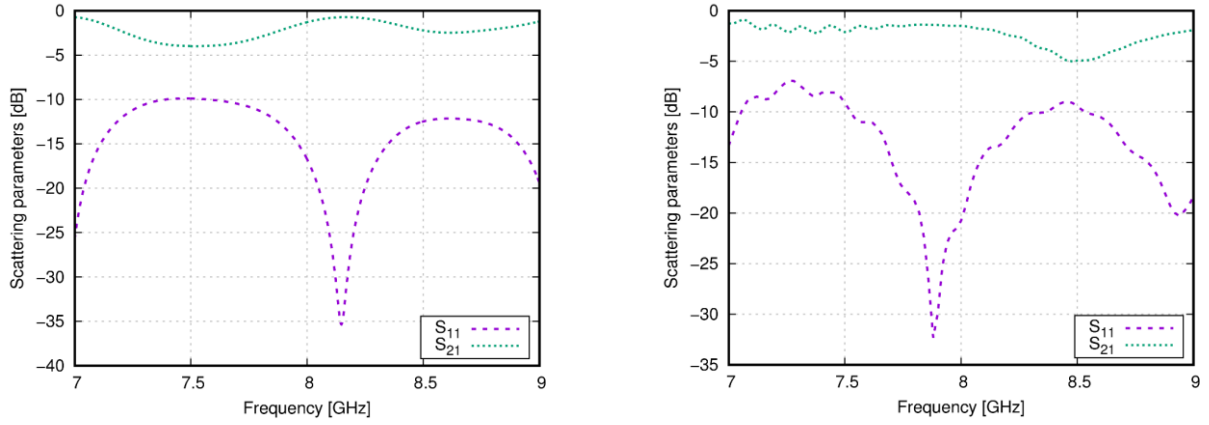


Figure 5 MTL-to-TIW transition for UWB band: simulated S parameters (left) and measured S parameters (right). Configuration from Figure 3.

3.4 CONCLUSIONS

The methodology of the design of multilayer transitions between MTL on a conventional substrate and TIW was presented. The designed transitions were simulated, and results were verified by measurements.

The conclusions are as follows:

- TIW can be used in combination with other devices integrated into other substrates.
- The presented MTL-to-TIW transition is suitable for narrow-band applications (for ISM bands, e.g.).
- The transition can be also used for wide-band applications with a higher insertion loss and a higher value of reflection coefficient.

4 TEXTILE INTEGRATED SWITCH

Since TIW are relatively bulky and are not suitable for wearable applications, attention is turned to non-wearable structures (bed sheets, upholstery, seat covers, etc.). In all those textile structures, TIW can play the role of a transmission line. TIW can be used as a high-speed communication bus for media streaming in cars, buses and airplanes. TIW-based systems can create a backup communication bus for sensors or emergency systems. The chapter is aimed to describe the design of a TIW switch, which is expected to transmit the power from the input 1 to the output 2, or the output 3.

The design of the textile-integrated T-divider is similar to the design of a SIW T-divider with some manufacturing limitations. The width of the waveguide is 35 mm for the operation frequency 5.8 GHz, the cutoff frequency $f_{\text{off}} = 3.9$ GHz and the 3D textile with the height 3.4 mm and the relative permittivity 1.2. The length of waveguide branches was chosen to be 20 mm.

4.1 SWITCH DESIGN AND SIMULATIONS

Schematics of the designed T-divider is depicted in Figure 6. The strong inductive post is in the vertical axis of the divider. On the left-hand side and the right-hand side, switchable pins to be used for switching are installed.

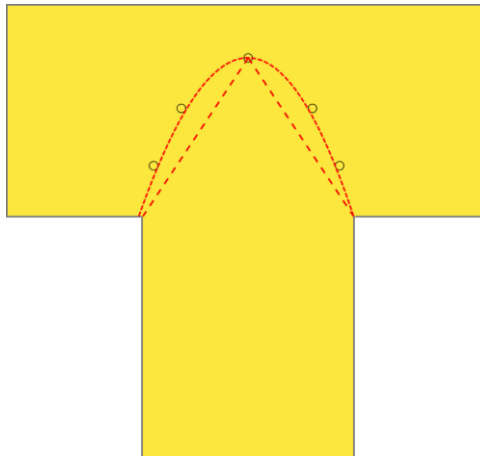


Figure 6 Position of the inductive post (on the top) and switchable pins (on the left, on the right). Linear or parabolic distribution.

The diameter and the conductivity of switchable pins are important as well. Therefore, all the switchable pins are constructed from copper wires. Switchable pins are placed inside the TIW. Their positions with respect to the central post and inner corners of the divider are given by an equilateral triangle or by a part of a parabolic curve (see Figure 6). The distances between pins are the same.

. Responses for closed ports are very similar for both the distributions, but responses for open ports are different: S_{11} is for about -19 dB better and S_{31} is for about 0.5 dB better in case of the parabolic distribution.

The shape of the gap between the inductive post and conductive layers is a circular ring slot (see Figure 8). The radius of the ring slot affects parameters of the switch. The top slot and the bottom one can have a different radius. Using a simplified model of the switch without PIN diodes (the diodes were replaced by a conductive strip), parametric analyses were done for the diameter of the top slot, and the diameter of the bottom slot.

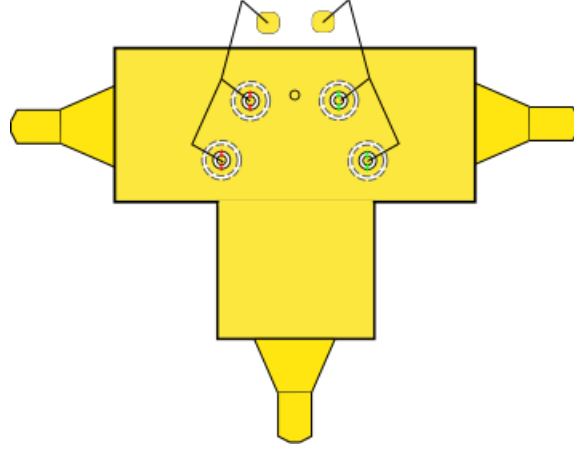


Figure 7 TIW switch with transitions to SMA connectors.

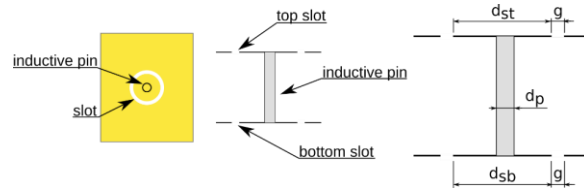


Figure 8 Design of switchable pins.

Table 2 shows that the diodes used in [13, 16] have lower capacitance and inductance than diodes used in [15], but these diodes are in a small package and cannot be used for textile manufacturing. Therefore, the PIN diodes BAR64-02 were used. Their maximum operation frequency is 6 GHz.

Table 2 Parameters of equivalent circuit components of PIN diodes.

PIN	$R_{ON} (\Omega)$	$R_{OFF} (k\Omega)$	C (pF)	L (nH)	Ref.
BAR64-02	2.1	3.0	0.20	0.80	[43]
HPND-4038	1.5	--	0.06	0.15	[41]
GC4941-12	1.5	--	0.06	--	[44]
MA4AGFCP910	5.0	--	0.02	--	[42]

. The switch with one PIN diode per pin had $S_{11} = -12.10$ dB, $S_{21} = -2.73$ dB and $S_{31} = -5.73$ dB. As shown in [13], one PIN diode per pin can be used, but parameters of used PIN diodes have to be much better than BAR64-02 has. Insertion loss of the open port is similar to cases with two and three PIN diodes. Due to the parallel combination of three PIN diodes, the switch has a very low transmission to the closed port (about -28.22 dB) but S_{11} is -17.12 dB. The switch with two PIN diodes has $S_{11} = -19.98$ dB but the transmission to the closed port is -23.25 dB.

4.2 SWITCH MANUFACTURING AND MEASUREMENTS

The TIW switch was designed for the 3D textile substrate 3D041 produced by SINTEX. The height of the 3D textile was 3.4 mm, relative permittivity 1.2 and the loss tangent $\tan \delta = 0.002$. Top and bottom conductive layers were screen-printed by a silver paste. The screen printing was chosen for the following reasons:

- The manufacturing process is compatible with the standard PCB technology.
- The precision of manufacturing is comparable to the standard PCB technology.
- The silver paste is well conductive.
- The PIN diodes or metal wires can be soldered or glued to the screen-printed silver paste.

The switch was measured using a two-port VNA. The VNA was connected by SMA connectors to the input port and one of the switchable ports. The unconnected port was ended by a $50\ \Omega$ resistor. Switchable pins were connected to the driving voltage $-5\ \text{V}$ for the open port (diodes OFF) and $+1.1\ \text{V}$ for the closed port (diodes ON). The current was limited by a series resistor to the maximum recommended value $80\ \text{mA}$. The manufactured switch is shown in Figure 9.

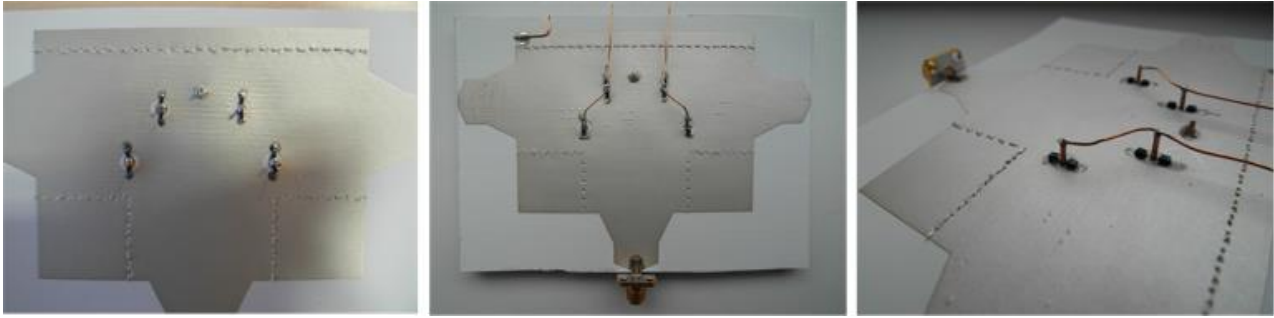


Figure 9 Photos of the screen-printed textile-integrated switch.

Simulated and measured results of the complete switch are depicted in Figure 10. The switch was simulated with SMA-to-TIW transitions and diodes replaced by the equivalent circuit. The reflection coefficient of the simulated switch was $-13.30\ \text{dB}$ (measured $-14.60\ \text{dB}$) at the frequency $5.8\ \text{GHz}$ and losses of the open port were $5.10\ \text{dB}$ (measured $6.21\ \text{dB}$). The simulated isolation of the closed port was $14.92\ \text{dB}$ (measured $15.63\ \text{dB}$). Obviously, measured data corresponds well with simulations.

4.3 CONCLUSIONS

The methodology of the design of the textile-integrated switch was presented in this Chapter. The design was verified by simulations and measurements. The design procedure can be divided into the following steps:

- The textile-integrated T-divider is designed with the fixed post in the longitudinal axis of the divider.
- Switchable conductive posts are installed into the divider following the linear or parabolic trajectory. The trajectory is defined by the center post and internal corners of the T-divider.
- Suitable PIN diodes are selected. The selection is limited by the operation frequency (parasite properties) and technology of creating metal layers.
- Top and bottom slots around switchable pins and the fixed post are designed. The bottom slots are recommended to be of the double size compared to top ones, approximately. The width of the slot is given by manufacturing technology (precision) and used PIN diodes. The parasitic properties of the diodes can be compensated by increasing the number of diodes.

These design rules were used for designing the textile-integrated switch for the ISM band $5.8\ \text{GHz}$. The switch was fed via SMA-to-TIW transitions by tapered microstrip lines on each port. Simulation shows that this transition was not ideal for this type of the textile material and degraded properties of the switch (see Figure 10).

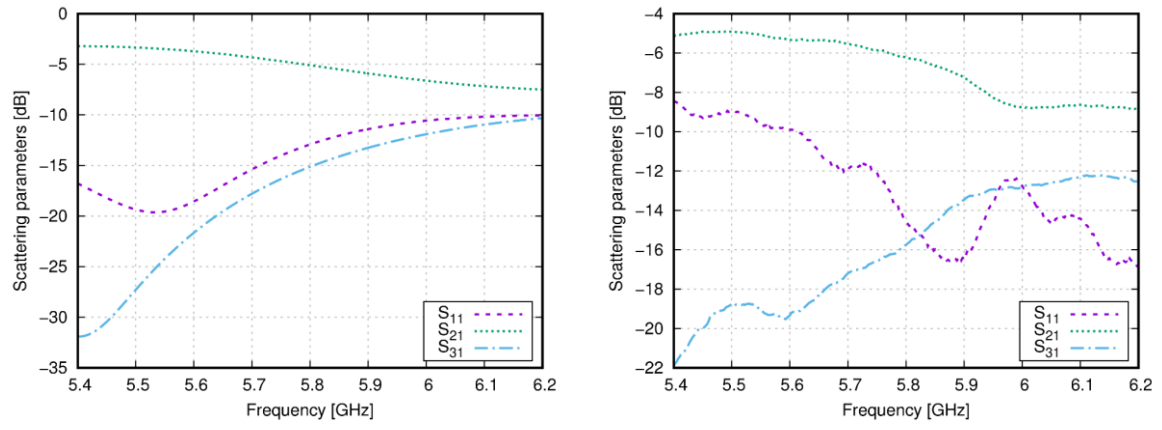


Figure 10 Frequency responses of S_{11} , S_{21} and S_{31} of the TIW switch: simulated (left) and measured (right).

5 CYRCULARLY POLARIZED TEXTILE-INTEGRATED ANTENNAS

The circularly polarized textile-integrated antenna is based on a concept of a circular patch antenna fed by the microstrip from the bottom side and with the cross slot inside the circular patch [27]. The role of the radiating element is played by a circular ring slot in the top metal layer of TIW. Inside the circular ring slot, a cross slot rotated for about 45° is etched to excite the circular polarization. The polarization of the antenna can be changed by the rotation of the cross slot.

The antenna is designed in two versions. The first version is more complicated for manufacturing at frequencies above 20 GHz, especially. The second version is easy to be manufactured because the most critical parts of the first version were eliminated. Hence, the second version is suitable even for higher frequencies above 20 GHz and a lower precision of manufacturing. Both versions of the antenna have similar properties; the first version has a better axial ratio (AR).

5.1 DESIGN OF TEXTILE-INTEGRATED ANTENNAS

The design of the antenna can be divided into two parts. First, the TIW has to be designed. Second, the radiating element has to be developed and its position has to be optimized. Design equations provide basic dimensions of radiating slots for further optimization.

The radiating element is depicted in Figure 11. The antenna consists of a circular ring slot and a cross slot inside. The circumference of the ring slot is given by the wavelength of the radiated wave. The circumference should equal to the wavelength of the radiated wave. The middle radius of the ring slot can be calculated by [28]:

$$r = \frac{c}{2\pi f_c \sqrt{\epsilon_r}} \quad (1)$$

where c is velocity of light in vacuum, f_c is frequency of operation and ϵ_r is relative permittivity of the textile substrate.

The width of the slot is given by the requested characteristic impedance of the slot.

The cross slot can be divided into two arms. The first arm is longer and the second one is shorter. The length of the longer arm is given by the radius of the circular ring slot and its width. There is a small conductive strip between the circular ring slot and these arms (see Figure 11). This thin strip improves the axial ratio of the antenna.

The length of the shorter arm is given by:

$$l_{e2} = r/4 \quad (2)$$

where r is the middle circumference of the ring slot given by (1).

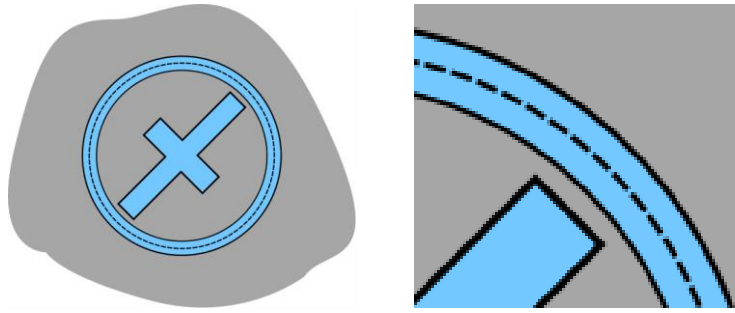


Figure 11 Version 1 of the radiating element (left), detail of the conductive strip between the ring slot and the cross slot (right).

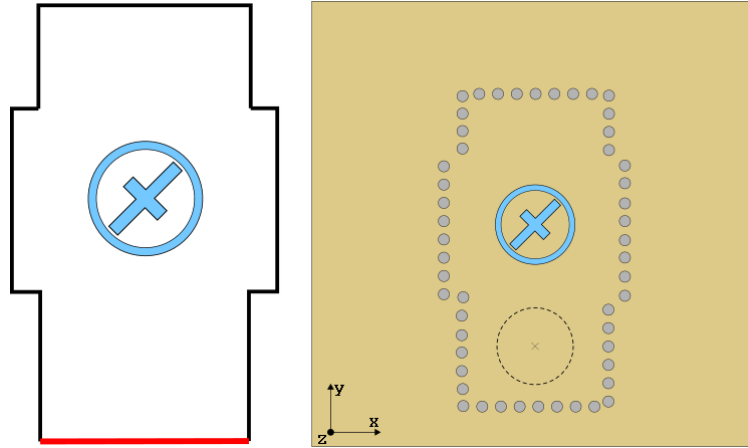


Figure 12 Version 1 of the antenna: simplified model (left), full model (right).

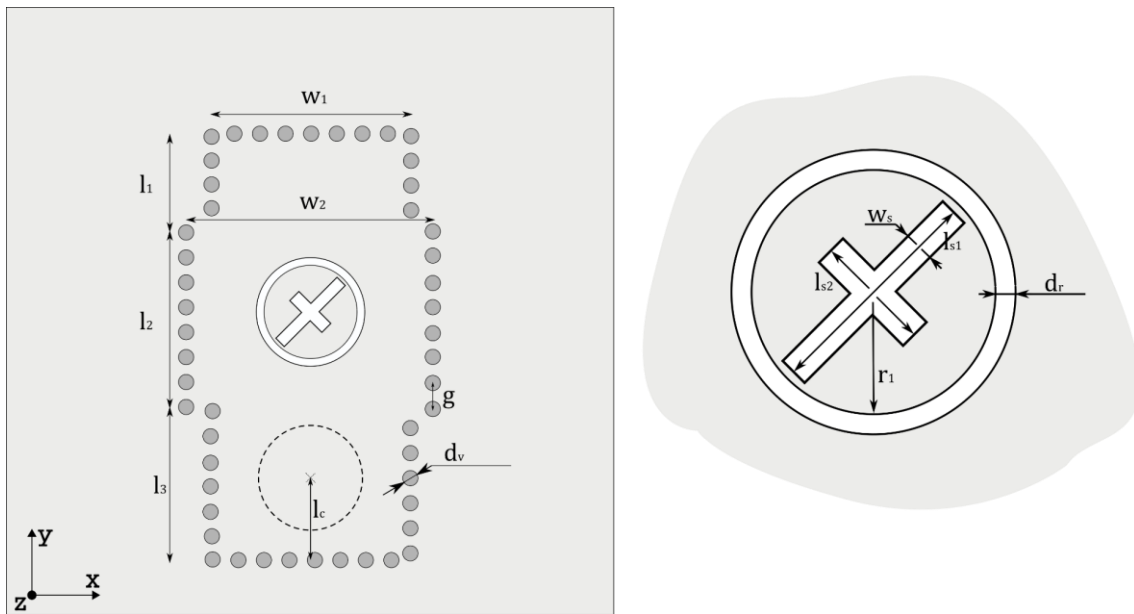


Figure 13 Version 1 of the textile-integrated antenna. The whole antenna (left), the radiating slot (right).

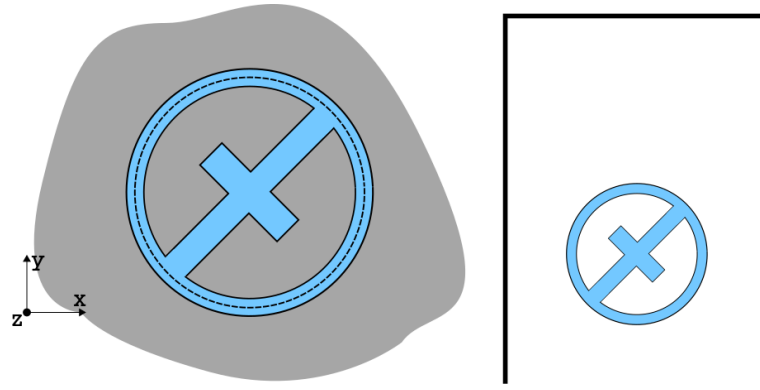


Figure 14 Version 2 of the radiating element with missing conductive strip (left), TIW feeder with unified width (right).

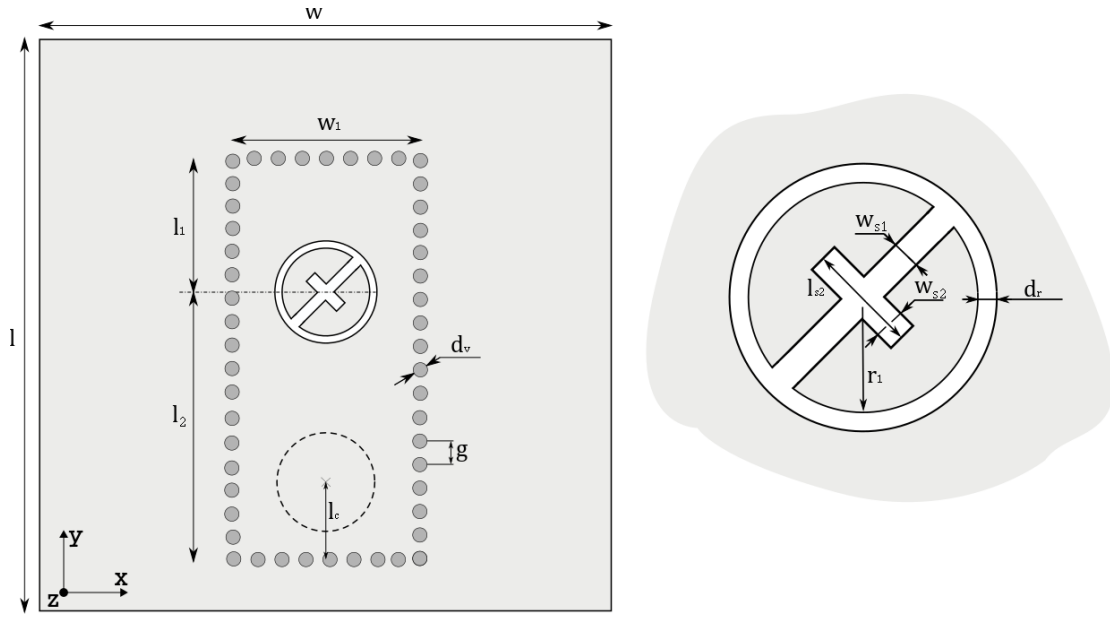


Figure 15 Version 2 of the textile-integrated antenna. The whole antenna (left), the radiating slot (right).

Table 3 Dimensions of version 2 of the textile-integrated antenna.

Param. [mm]	l_1	l_2	w_1	d_v	g	l_c	w_{s1}	w_{s2}	l_{s2}	r_1	d_r
5.8 GHz	25.8	55.7	40.82	0.3	1.2	22.6	2.5	2.7	12.3	9.8	2.5
24 GHz	5.86	11.30	10.20	0.3	1.2	3.23	0.42	1.28	1.79	1.76	0.65

Table 4 Dimensions of version 1 of the textile-integrated antenna.

Param. [mm]	l_1	l_2	l_3	w_1	w_2	d_v	g	l_c	w_{s1}	w_{s2}	l_{s1}	l_{s2}	r_1	d_r
24 GHz	6.00	7.00	3.93	7.74	9.70	0.30	1.00	3.23	0.46	0.51	3.40	1.75	1.85	0.27

5.2 SIMULATION, IMPLEMENTATION AND MEASUREMENT OF TIW ANTENNAS

Version 1: simulation

The antenna was simulated in CST Microwave Studio. Simplified simulations considered continuous metal sidewalls of TIW and feeding by a waveguide port connected to TIW directly (the red line in Figure 12). The antenna was optimized for resonance frequency 24 GHz and axial ratio lower than 3 dB in the frequency range from 24.00 GHz to 24.25 GHz.

The frequency response of the reflection coefficient of the simulated version 1 antenna with full sidewalls and the waveguide port connected directly to the waveguide is depicted in Figure 16. The impedance bandwidth of the antenna for $S_{11} < -10$ dB is 11.05 % (23.18 GHz to 25.83 GHz).

The AR bandwidth of the version 1 (see Figure 17) is lower than the impedance bandwidth, reaches 327 MHz and covers the whole ISM band. The antenna was not optimized for the best parameters because the model is strongly simplified.

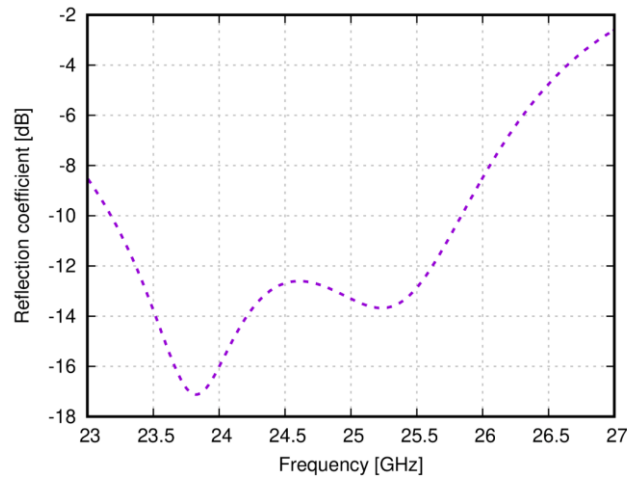


Figure 16 Simulated frequency response of reflection coefficient of the version 1 antenna: continuous walls and waveguide port.

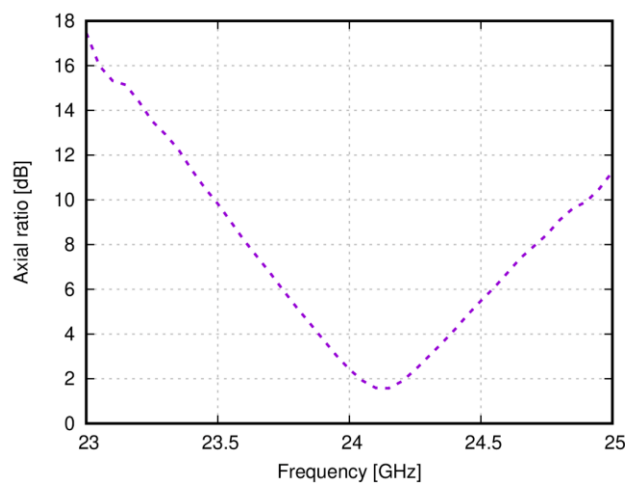


Figure 17 Simulated frequency response of axial ratio of the version 1 antenna: continuous walls and waveguide port.

Radiation patterns of the version 1 antennas are shown in Figure 18. The width of the main lobe is 101° in the XZ plane and 100.7° in the YZ plane. The maximal gain is 6.61 dBi and the maximum is shifted to directions 17° and 23° . The gain in the front direction is 5.53 dBi.

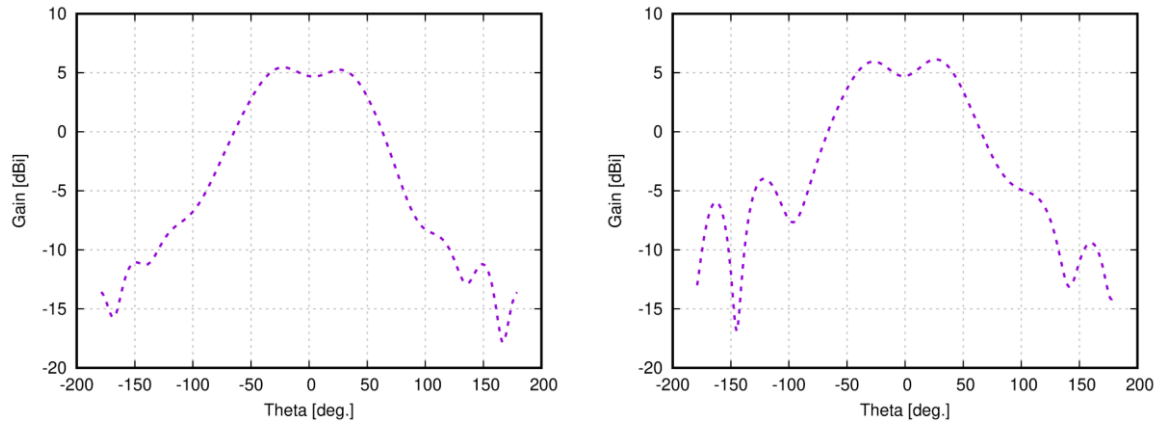


Figure 18 Simulated radiation patterns of the version 1 antenna with the waveguide port: XZ plane (left) and YZ plane (right).

Version 1: implementation and measurement

The antenna was fabricated from the 3D knitted fabric 3D097 produced by SINTEX. The relative permittivity of the fabric was 1.2 and the height was 2.6 mm. The conductive metal layers were manufactured by the PCB technology from a self-adhesive copper foil (the thickness 0.03 mm). The PCB technology allowed to achieve a good manufacturing precision which is important at the operation frequency 24 GHz.

The sidewalls of TIW were sewed by the conductive thread ELITEX 440 dtex produced by IMBUT. The resistivity of the thread was 15.52Ω (for details, see Chapter 6). The precise connector was soldered to the bottom conductive copper foil. Photography of the manufactured antenna is depicted in Figure 19.

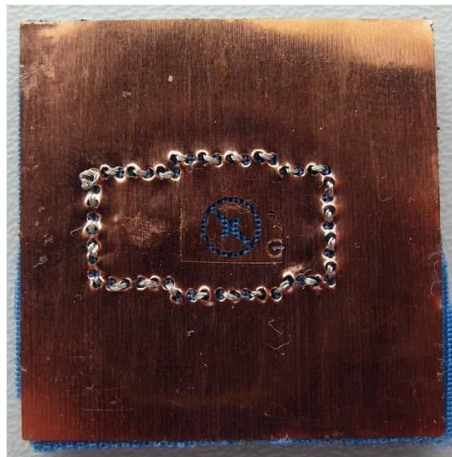


Figure 19 Photograph of the version 1 antenna for the ISM band 25 GHz; manufactured from copper foil

Figure 20 shows that the measured value of reflection coefficient decreased for about 4 dB with respect to simulation. The bandwidth of the antenna was 800 MHz. This decrease was caused by a combination of several factors:

- Additional losses are given by conductivity of the used thread,
- Additional losses are given by humidity in the knitted fabric,
- The simulation model did not contain all changes of dimensions caused by under-etching.

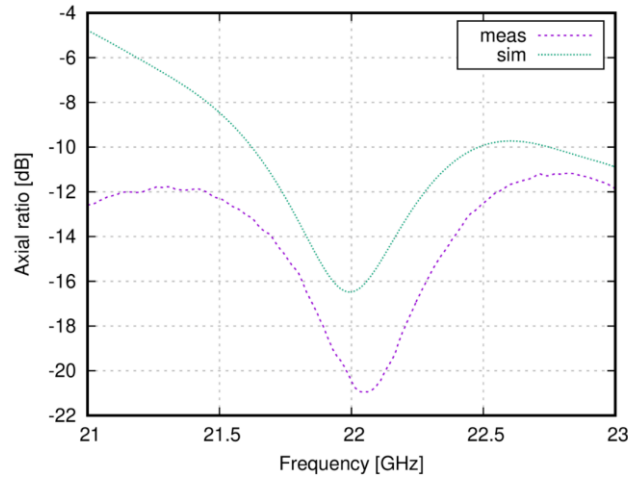


Figure 20 Version 1 antenna for the ISM band 25 GHz:
simulated and measured frequency response of reflection coefficient.

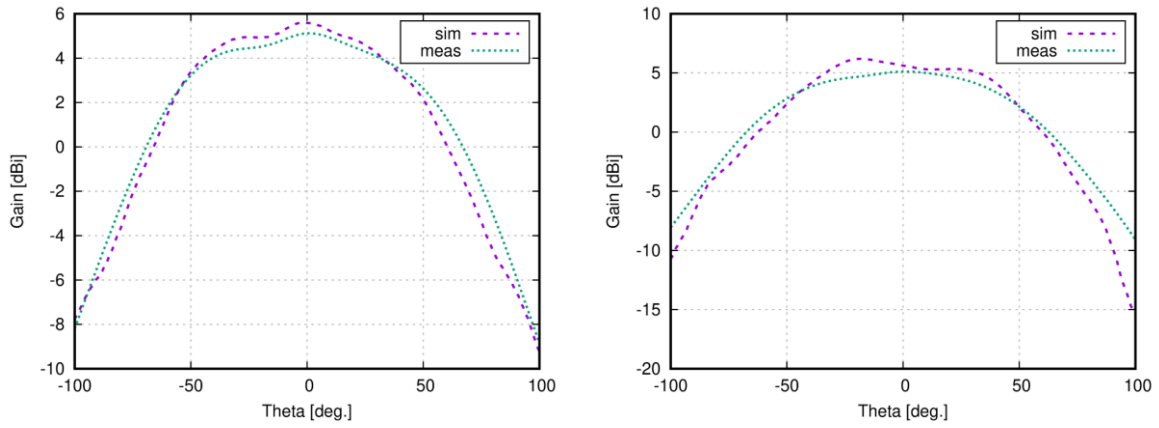


Figure 21 Version 1 antenna for the ISM band 25 GHz:
simulated and measured radiation patterns in XZ plane (left) and YZ plane (right).

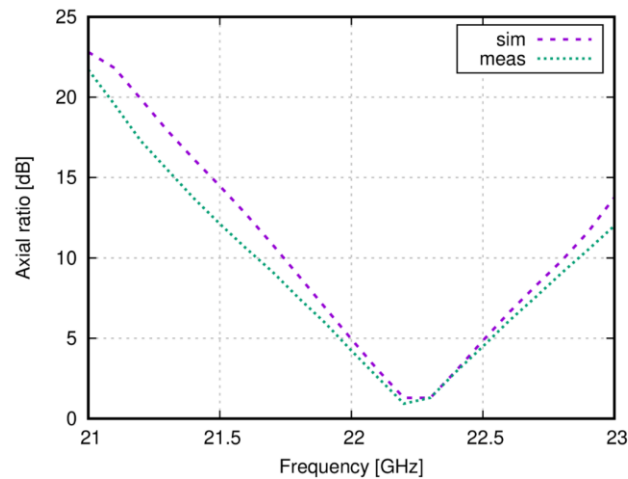


Figure 22 Version 1 antenna for the ISM band 25 GHz:
simulated and measurement frequency response of axial ratio.

Radiation patterns and the gain of the antenna are shown in Figure 21. The measured gain is 5.81 dBi at the frequency 22.20 GHz and the main lobe width in the XZ plane is 112° and in the YZ plane is 91° . Due to the configuration of the anechoic chamber, radiation patterns were measured only in the span from -100° to

100° in both planes. Figure 22 shows frequency response of the axial ratio of the version 1 antenna. The minimal value of the AR is 0.93 dB at the frequency 22.20 GHz and the AR bandwidth is 386 MHz.

Version 2: simulations

The version 2 of the antenna was designed at two frequencies. The first one was the ISM band 5.8 GHz and the second one the ISM band 24 GHz. Both the antennas were designed by same procedure and optimized for typical impedance and axial ratio bandwidths and maximal radiation in the front direction.

Figure 23 shows frequency response of the reflection coefficient and the axial ratio in the Z direction. The impedance bandwidth of the antenna is wider than the depicted 2 GHz and is similar to the version 1 of the antenna.

The minimum of the axial ratio is 1 dB and the frequency of the minimum is 24 GHz. There are small differences between responses provided by the frequency-domain solver and the time-domain solver. These differences can be caused by differences in meshes and solver errors. The axial ratio bandwidth is 967 MHz (T-solver) and 959 MHz (F-solver).

Radiation patterns are shown in Figure 24. The main lobe width is 104.7° in the XZ plane and 105.2° and in the YZ plane. The simulated gain of the antenna is 6.37 dBi and the main direction of the maximum is 4° in the XZ plane and 5° in the YZ plane. The front to back ratio of the antenna is 28.25 dB.

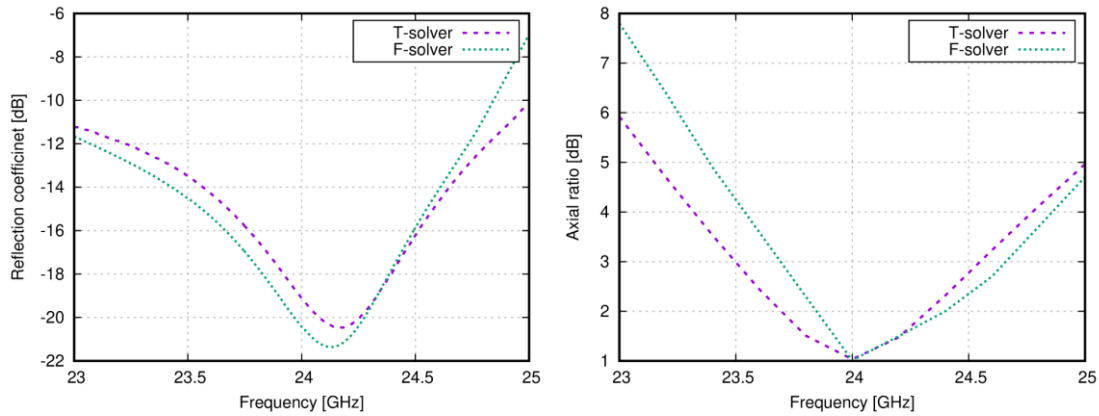


Figure 23 Frequency responses of reflection coefficient (left) and axial ratio (right) of version 2 antenna for the ISM band 24 GHz.

Time-domain solver versus frequency-domain solver

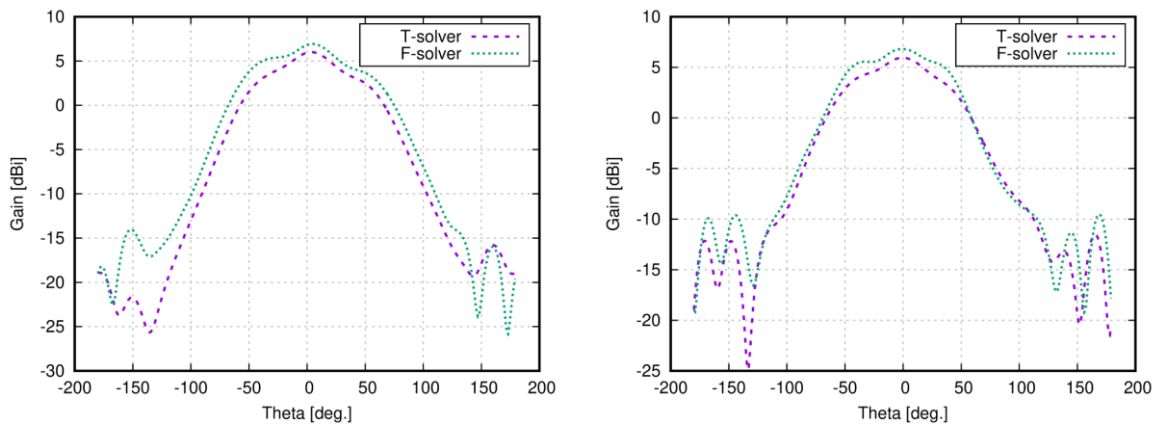


Figure 24 Radiation patterns of version 2 antenna at 24 GHz: the XZ plane (left), the YZ plane (right).

Version 2: implementation and measurement

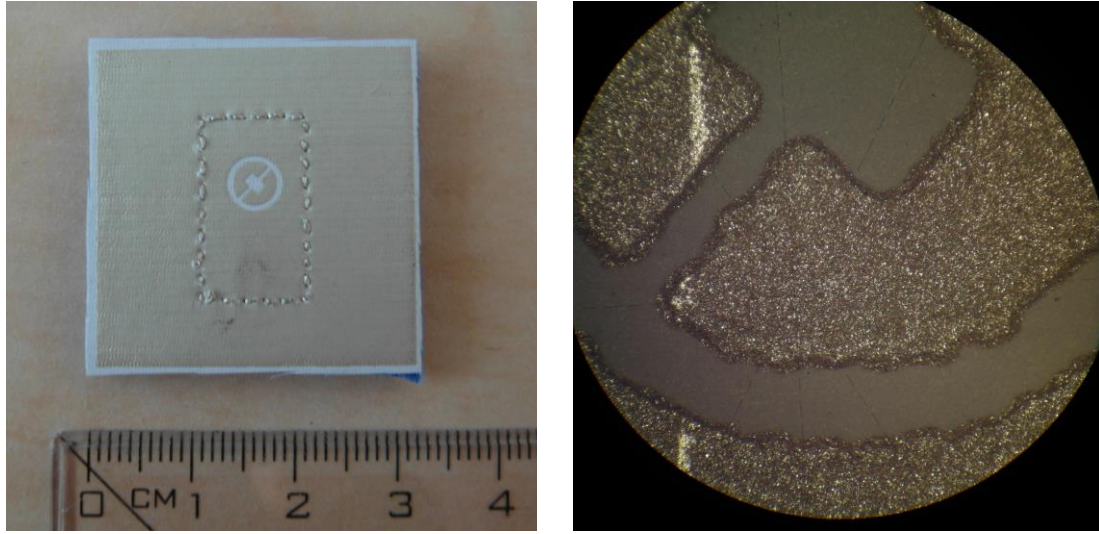


Figure 25 Photograph of the version 2 screen-printed antenna for the ISM band 24 GHz: the macroscopic view (left), the microscopic view (right).

The antenna was printed on the DIGIFLEX MASTER foil by a silver polymer paste. In Figure 25, the macroscopic photo (left) and the microscopic one (right) are given. Since the viscosity of the polymer paste is not high enough, the shape of the antenna layout is not sharp, and the width of the ring slot is not constant.

Measured frequency responses of the reflection coefficient and the axial ratio are shown in Figure 26. The minimum of reflection coefficient is shifted to the frequency 22.7 GHz and the shape differs from the copper antenna and the simulation. The impedance bandwidth of measured printed antenna is 3.02 GHz. Since the resonant frequency is shifted to lower frequency, also the minimum of the axial ratio is shifted to the frequency 22.25 GHz. The minimum magnitude of the axial ratio is 1.06 dB. The axial ratio bandwidth is 1.2 GHz. Radiation patterns are shown in Figure 27 for the XZ plane and the YZ plane. The maximum of the gain declines for about -2° and -4° , respectively. The maximum gain is 4.2 dBi. The radiation patterns are measured in the minimum of the axial ratio (22.25 GHz). The width of the main lobe is 79° in the YZ plane and 95° in the XZ plane.

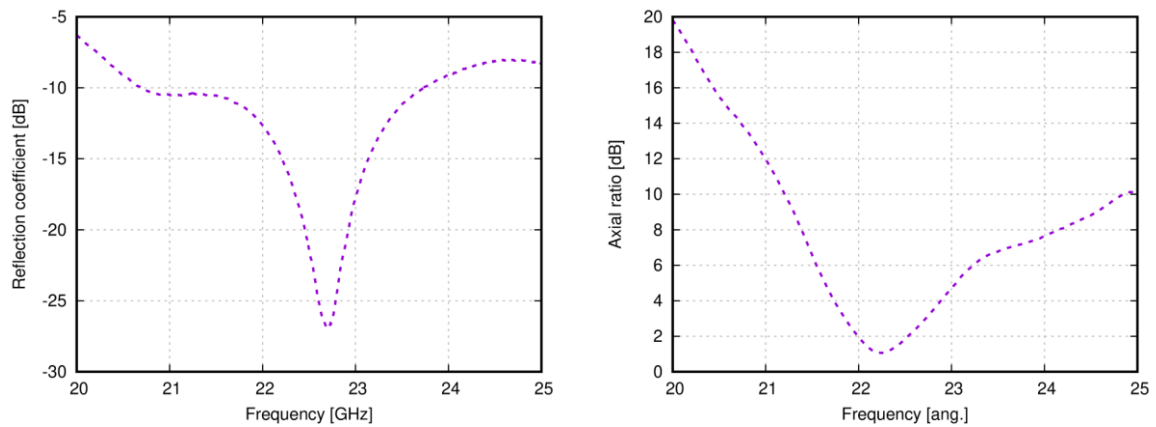


Figure 26 Measured frequency response of reflection coefficient (left) and axial ratio (right) of version 2 antenna for ISM band 24 GHz (screen printing).

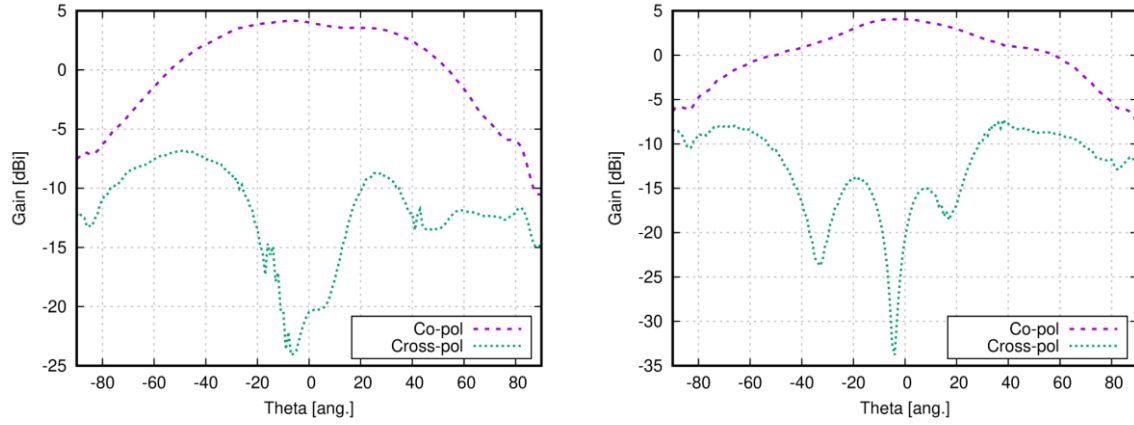


Figure 27 Measured radiation patterns of version 2 antenna for ISM band 24 GHz (screen printing) at 22.25 GHz: YZ plane (left); XZ plane (right).

5.3 CONCLUSIONS

Two versions of the circularly polarized slot antenna were presented in this chapter. The First version of the antenna has been designed for ISM band 24 GHz and compared simulated and measured results. Due to manufacturing under-etching, the resonance frequency of the antenna shifted to 22.3 GHz. The second version of the antenna was simplified and prepare for manufacturing by screen printing technology. Two versions of the antenna were manufactured. The first one was designed for ISM 5.8 GHz and the second for ISM band 24 GHz.

The resonance frequency of manufactured ISM 5.8 GHz antenna is shifted to lower frequency because the antenna was simulated without interlayer used for printing.

The version 2 of the antenna designed for the ISM band 24 GHz was manufactured using both the copper foil and screen printing. Both versions of the antenna were measured and compared with simulated data. The copper antenna is well matched at the frequency 24 GHz but the axial ratio is about 5 dB in the minimum. The resonant frequency of the screen-printed antenna is shifted to 22.7 GHz.

6 TECHNOLOGICAL ASPECTS

The technological aspects of manufacturing mm-wave structures on textile substrates have specific features comprising used materials, technologies and their precision which is about $\pm 10\%$ in the textile industry. Parameters of textile materials used as substrates, conductive surfaces or threads are given with a typical precision which is relatively low. Since the thesis deal with the design of TIW-based components and antennas, there are three main conductive objects to be characterized: textile substrates, conductive surfaces and conductive sidewalls.

3D textile materials, which are used as substrates in this work, were measured by the transmission line method and presented in [29]. Values of relative permittivity of selected textile substrates are shown in **Table 5**

Table 5 Materials properties of selected 3D textile substrates.

Material	Relative permittivity	Losses ($\tan \delta$)
3D041	1.22	0.0021
3D097	1.22	0.0019

Conductive surfaces are another interesting component of textile-integrated antennas and circuits. As described in the *State of the Art*, two manufacturing techniques are used in the thesis:

- **The self-adhesive copper foil.** The layout can be prepared compatibly with the standard PCB technology with the comparable precisions. The thickness of the copper foil is 0.035 mm and the glue is on its bottom side.
- **Screen printing.** A silver paste can be printed by screen printing technology to various surfaces (textiles, foams, etc.). Since the used 3D textile is porous, the silver paste penetrates into the textile substrate and does not create a conductive surface on the top of the textile only. Therefore, an iron-on foil is used to avoid the penetration of the silver paste and to smoothen the textile surface before printing. Thickness of the foil is 0.08 mm and relative permittivity 2.1. A corresponding layer has to be added to the simulation model to prevent shift of the resonant frequency.

6.1 CONDUCTIVE THREADS

Conductive threads can be manufactured from different materials, with different thicknesses and conductivities. Conductive threads are usually composed from two types of materials – from a non-conductive fiber (cotton, polyester, etc.) and a conductive wire (silver, stainless steel, carbon, but also copper, nickel, etc.). Conductive threads are usually classified according to a used conductive material:

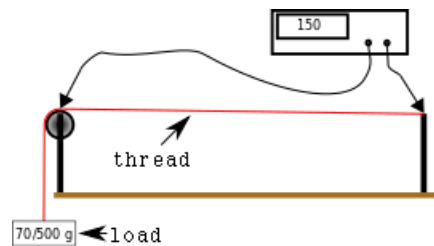
- **Carbon** (threads no. 1 and 11 in **Table 6**). Threads are dominantly used for protective clothes and EM shielding.
- **Stainless steel** (threads no. 2, and 7 to 10 in **Table 6**). Threads are manufactured from textile fibers and thin steel wires. Threads show a better conductivity compared to carbon threads.
- **Silver threads** (threads no. 3 to 6, and 12 to 15 in **Table 6**). Threads are manufactured from textile fibers which are enriched by silver particles. Silver threads show a very good conductivity even for a very thin thread (the diameter ~ 0.3 mm).

Table 6 List of measured threads.

No.	Materials	Name	Linear mass density	Datasheet resistivity	Manufacturer
1.	PAD/carbon	F901	144 dtex		Shakespeare
2.	Stainless steel	Bekonix VN 14.1.9.00Z	110 tex	70	Bekaert
3.	PAD/silver	silver-stat	240 dtex	---	R-stat
4.	PAD/silver	X-static	160 dtex	---	NFT
5.	PAD/silver	Elitex 220 dtex	220 dtex	70	Imbut
6.	PAD/silver	Elitex 440 dtex	440 dtex	20	Imbut
7.	Stainless steel	Bekonix VN 12.1.2. 100Z	235 dtex	30	Bekaert
8.	Stainless steel	Bekonix VN 12.3..2.175S	760 dtex	9	Bekaert
9.	PES/Stainless steel	Bekonix BK 50/3	50/3Nm	---	Bekaert
10.	PES/Stainless steel	I-tech 20	312*3 dtex	---	Amann
11.	PES/Carbon	C-tech 80	111*3 dtex	---	Amann
12.	Silver	Schildtex 235f	560 dtex	<100	Statex
13.	PAD/Silver	Shieldtex 110/34 dtex HC	10/34 dtex	<3000	Statex
14.	PAD/Silver	Shieldtex 110/34 dtex HC	117/17 dtex	<3000	Statex
15.	PAD/Silver	Silver-tech 120	90*3 dtex	360	Amann

6.2 MEASUREMENT OF THREADS AND RESULTS

Conductive threads are produced by different manufacturers from different materials with various thicknesses. Obviously, mechanical parameters (elasticity) and electrical parameters (resistance) of those threads differ. Some threads can change its resistance depending on the tension (which is used for sensing mechanical tension or breath).

**Figure 28** Measurement of threads.

The threads were measured by the RLC meter LCR-819 between two points (see Figure 28). The threads were stretched by loads 70 g and 500 g.

Table 7 Measured resistivity of conductive threads.

	70 g				500 g			
	DC	1 kHz	10 kHz	100 kHz	DC	1 kHz	10 kHz	100 kHz
1.	7.7 M	2.54 M	2.5 M	697.7 k	-----	-----	-----	-----
2.	73.33	68.92	68.9	69.72	69.61	68.94	68.96	69.42
3.	226	228.8	228.6	229.4	234	232	232.2	233.2
4.	232	255.4	254.6	254.6	-----	-----	-----	-----
5.	72.26	72.42	74.92	63.60	NA	NA	NA	NA
6.	14.08	14.22	14.25	14.30	15.52	15.56	15.70	15.68
7.	50	36.2	37.46	31.8	38	29.88	29.8	29.86
8.	11	9.23	9.18	9.32	10.8	9.18	9.19	9.25
9.	3 k	4.04 k	2.228 k	13.34 k	1.6 k	1.904 k	1.666 k	1.53 k
10.	7 k	3.26 k	3.82 k	2.394 k	2.5 k	2.394 k	2.34 k	2.626 k
11.	> 200 M	>200 M	75.78 M	0.5 M	> 200 M	> 200 M	53.2 M	> 200 M
12.	15	13.88	13.95	13.95	14.11	13.32	13.64	13.67
13.	758	848	823.2	743	643	594.32	633	652
14.	141	140.8	140.5	140.24	148.1	149.8	149.6	149.8
15.	309	305.60	305.40	304	311	308	310	310

The threads 2, 5, 6, 7, 8 and 12 were selected to create the sidewalls of SIW, and the SIW was simulated in CST Microwave Studio. SIW was not optimize for the best S_{21} but it is only as a testing example. The cutoff frequency was s 5 GHz. The simulated results are shown in Figure 29. The transmission coefficient varies between -2 dB and -3 dB.

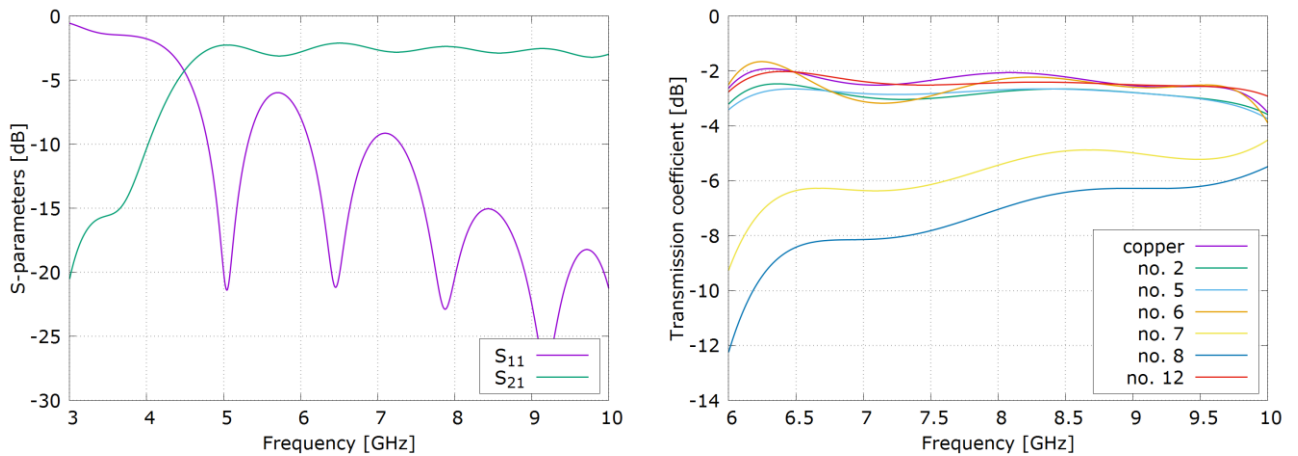


Figure 29 Simulated SIW characteristics for testing conductive threads (left). Frequency response of transmission coefficient of SIW with sidewalls created from conductive threads (right).

6.3 CONCLUSIONS

The resistivity of fifteen conductive threads was measured and some threads were tested as sidewalls of SIW. The threads were loaded by two loads during the resistivity measurement to achieve the same conditions for threads. Threads were measured by an RLC meter at four different frequencies. Threads, which have resistance lower than 100 Ohms, were used as sidewalls of SIW. This practical test shows that threads with a low DC resistivity are not any time the best choice for this type of application and the selection depend on the material of the thread and its construction.

For manufacturing TIW structures, threads no. 6 and 12 can be recommended. Both threads are PAD/silver based with a relatively high linear mass density, but the diameter of the thread number 6 is 0.3 mm and the diameter of the thread number 12 is 1 mm. Due to this reason, the thread no. 6 is suitable for more applications, machine sewing and hand sewing.

7 SUMMARY

The dissertation thesis was aimed to extend possibilities of textile-integrated electronics. Attention was turned to high frequency circuits integrated into textile substrates, especially. The basic concepts of planar antennas and circuits were advanced to ensure a reliable operation in ISM bands 5.8 GHz and 24 GHz, and the band group 6 UWB band.

Textile-integrated electronics has been intensively researched for last 30 years. Nevertheless, only few products based on textile-integrated electronics is commercially available to operate without a plastic box or another protection. Research outputs in field of textile-integrated electronics are interesting but manufacturing and integration are difficult and expensive. Last but not least, the problems with durability of textile-integrated electronics in clothing have not been solved yet sufficiently. But clothing is not the only application field of textile-integrated electronics. Promising applications of textile-integrated electronics appear also in the area of homecare systems and vehicles.

In the thesis, attention is turned to vehicular applications (cars, busses, airplanes). Thanks to the textile-integrated electronics, purely textile upholstery and seat covers can obtain additional functions. The upholstery-integrated electronics can be:

- Relatively large because textile materials cover relatively large surfaces;
- Durable because upholstery is not washed and is protected by a cover layer (glass-laminate panels in airplanes);
- Reliable because integrated communication busses or sensor networks are supported by a planar, firm surface of a vehicle.

The role of the main building block of textile-integrated electronics is played by textile-integrated waveguides (TIW). In the *State of the Art*, the progress in the TIW-based integration of microwave components was documented, and particular manufacturing options were discussed comprising screen printing, inkjet printing and embroidering. In order to create side walls of TIW, various approaches were presented including metal eyelets, conductive threads or conductive textiles. Advanced circuits were shown to be implemented by the combinations of conventional substrates, integrated buttons and elementary semiconductor elements.

The PhD thesis was aimed to meet three main objectives:

Objective 1

The methodology of designing the transition between a microstrip line on a conventional substrate and a textile-integrated waveguide was presented in Chapter 3. The transition was constructed using a current probe placed into the waveguide. The transition is similar to the transition between a coaxial connector and a SIW.

In the thesis, two transitions were proposed. The first transition was optimized for the ISM frequency band 5.8 GHz and the second one for the UWB frequency band 8 GHz. Results indicate that the transitions are suitable for narrowband applications. The attenuation of transitions (including SMA connectors) was 3.32 dB for the 5.8 GHz ISM band and varied from 1.1 dB to 4.3 dB for in the band group 6 UWB band.

Objective 2

The methodology of designing a textile-integrated waveguide switch was presented in Chapter 4. The switch was based on a T divider completed by PIN diodes playing the role of control elements. The divider was optimized for the textile integration. Achieved parameters were worse than those available in [41, 42]. This result was caused by larger manufacturing tolerances, by the use of PIN diodes with a larger package and stronger parasitic properties. The improper transition between the SMA connector and the TIW is another disadvantage.

The divider was designed for the working frequency 5.8 GHz and was manufactured by screen printing. The following parameters were measured: reflection from the input port -14.60 dB, transmission to the open port -6.21 dB and transmission to the closed port -14.92 dB.

Objective 3

The methodology of designing a circularly polarized antenna for operation frequencies 5.8 GHz and 24 GHz was described in Chapter 5. Two versions of the antenna were implemented – the first one was manufactured using a copper foil and the second one was produced by screen-printing. Properties of both the antennas were experimentally verified. Antennas achieved gains ranging from 4 to 6 dBi. The circular polarization of the antennas was proven by measuring the axial ratio, which was 1 dB in the minimum.

In case of antennas optimized for the frequency 24 GHz and manufactured by screen printing, the resonant frequency was shifted due to the manufacturing limitations.

8 REFERENCES

- [1] HUGHES-RILEY, T., DIAS, T., CORK, C. A Historical Review of the Development of Electronic Textiles. *Fibers* [online]. 2018, **6**(2), 34. doi: 10.3390/fib6020034
- [2] LI, Y., TORAH, R., BEEBY, S. P., TUDOR, J. Inkjet printed flexible antenna on textile for wearable applications. 2012.
- [3] KRYKPAYEV, B., FAROOQUI, M., BILAL, R. M., VASEEM, M., SHAMIM, A. A wearable tracking device inkjet-printed on textile. *Microelectronics Journal* [online]. 2017, **65**, 40–48. ISSN 0026-2692. doi: 10.1016/j.mejo.2017.05.010
- [4] BOZZI, M., MOSCATO, S., SILVESTRI, L., DELMONTE, N., PASIAN, M., PERREGRINI, L. Innovative SIW components on paper, textile, and 3D-printed substrates for the Internet of Things. In: *2015 Asia-Pacific Microwave Conference (APMC)* [online]. 2015, p. 1–3. doi: 10.1109/APMC.2015.7411615
- [5] MORO, R., BOZZI, M., AGNEESSENS, S., ROGIER, H. Compact cavity-backed antenna on textile in substrate integrated waveguide (SIW) technology. In: *2013 European Microwave Conference* [online]. 2013, p. 1007–1010. doi: 10.23919/EuMC.2013.6686830
- [6] MORO, R., AGNEESSENS, S., ROGIER, H., DIERCK, A., BOZZI, M. Textile Microwave Components in Substrate Integrated Waveguide Technology. *IEEE Transactions on Microwave Theory and Techniques* [online]. 2015, **63**(2), 422–432. ISSN 0018-9480, 1557-9670. doi: 10.1109/TMTT.2014.2387272
- [7] VASINA, P., LACIK, J. Textile linear polarization reconfigurable ring slot antenna for 5.8 GHz band. In: *2017 Conference on Microwave Techniques (COMITE)* [online]. 2017, p. 1–4. doi: 10.1109/COMITE.2017.7932311
- [8] KAUFMANN, T., XU, Z., FUMEAUX, C. Wearable substrate-integrated waveguide with embroidered vias. In: *The 8th European Conference on Antennas and Propagation (EuCAP 2014)* [online]. 2014, p. 1746–1750. doi: 10.1109/EuCAP.2014.6902130
- [9] MORO, R., AGNEESSENS, S., ROGIER, H., BOZZI, M. Wearable textile antenna in substrate integrated waveguide technology. *Electronics Letters*. 2012, **48**(16), 985–987.
- [10] LEMEY, S., AGNEESSENS, S., ROGIER, H. Textile SIW antennas as hybrid energy harvesting and power management platforms. In: *2015 European Microwave Conference (EuMC)* [online]. 2015, p. 20–23. doi: 10.1109/EuMC.2015.7345689
- [11] KAUFMANN, T., FUMEAUX, C. Wearable Textile Half-Mode Substrate-Integrated Cavity Antenna Using Embroidered Vias. *IEEE Antennas and Wireless Propagation Letters* [online]. 2013, **12**, 805–808. ISSN 1536-1225. doi: 10.1109/LAWP.2013.2270939
- [12] WEI, S., YANG, C., CHEN, Y., CHEN, T., CHANG, C. \sqrt{V} - and \sqrt{W} -Band Substrate Integrated Waveguide (SIW) Mechanical Switch. *IEEE Transactions on Microwave Theory and Techniques* [online]. 2018, **66**(6), 3090–3098. ISSN 0018-9480. doi: 10.1109/TMTT.2018.2825381
- [13] LIM, I., LIM, S. Substrate-Integrated-Waveguide (SIW) Single-Pole-Double-Throw (SPDT) Switch for X-Band Applications. *IEEE Microwave and Wireless Components Letters* [online]. 2014, **24**(8), 536–538. ISSN 1531-1309. doi: 10.1109/LMWC.2014.2321065

- [14] NUMAN, A. B., FRIGON, J., LAURIN, J. Single-Pole Single-Throw Switch for Substrate-Integrated Waveguide. *IEEE Microwave and Wireless Components Letters* [online]. 2018, **28**(3), 221–223. ISSN 1531-1309. doi: 10.1109/LMWC.2018.2804259
- [15] XU, R. F., IZQUIERDO, B. S., YOUNG, P. R. Switchable Substrate Integrated Waveguide. *IEEE Microwave and Wireless Components Letters* [online]. 2011, **21**(4), 194–196. ISSN 1531-1309. doi: 10.1109/LMWC.2011.2108274
- [16] CHEN, H., CHE, W., ZHANG, T., CHAO, Y., FENG, W. SIW SPDT switch based on switchable HMSIW units. In: *2016 IEEE International Workshop on Electromagnetics: Applications and Student Innovation Competition (iWEM)* [online]. 2016, p. 1–3. doi: 10.1109/iWEM.2016.7504980
- [17] KLEMM, M., LOCHER, I., TROSTER, G. A novel circularly polarized textile antenna for wearable applications. In: *7th European Conference on Wireless Technology, 2004*. 2004, p. 285–288.
- [18] RAIS, N. H. M., SOH, P. J., MALEK, F., AHMAD, S., HASHIM, N. B. M., HALL, P. S. A review of wearable antenna. In: *2009 Loughborough Antennas Propagation Conference* [online]. 2009, p. 225–228. doi: 10.1109/LAPC.2009.5352373
- [19] PINAPATI, S. P., KAUFMANN, T., LINKE, I., RANASINGHE, D., FUMEAUX, C. Connection strategies for wearable microwave transmission lines and antennas. In: *2015 International Symposium on Antennas and Propagation (ISAP)*. 2015, p. 1–4.
- [20] CHEN, S. J., KAUFMANN, T., RANASINGHE, D. C., FUMEAUX, C. A Modular Textile Antenna Design Using Snap-on Buttons for Wearable Applications. *IEEE Transactions on Antennas and Propagation* [online]. 2016, **64**(3), 894–903. ISSN 0018-926X. doi: 10.1109/TAP.2016.2517673
- [21] SEAGER, R. D., FLINT, J. A., FONSECA, D. S. Textile-to-rigid microstrip transition using permanent magnets. *Electronics Letters* [online]. 2015, **51**(9), 709–710. ISSN 0013-5194, 1350-911X. doi: 10.1049/el.2014.4361
- [22] SUNTIVES, A., ABHARI, R. Transition Structures for 3-D Integration of Substrate Integrated Waveguide Interconnects. *IEEE Microwave and Wireless Components Letters* [online]. 2007, **17**(10), 697–699. ISSN 1531-1309. doi: 10.1109/LMWC.2007.905592
- [23] CHAHAT, N., ZHADOBOV, M., MUHAMMAD, S. A., COQ, L. L., SAULEAU, R. 60-GHz Textile Antenna Array for Body-Centric Communications. *IEEE Transactions on Antennas and Propagation* [online]. 2013, **61**(4), 1816–1824. ISSN 0018-926X. doi: 10.1109/TAP.2012.2232633
- [24] LOCHER, I., KLEMM, M., KIRSTEIN, T., TRSTER, G. Design and Characterization of Purely Textile Patch Antennas. *IEEE Transactions on Advanced Packaging* [online]. 2006, **29**(4), 777–788. ISSN 1521-3323. doi: 10.1109/TADVP.2006.884780
- [25] POZAR, D. M. *Microwave Engineering*. 4 edition. Hoboken, NJ: Wiley, 2011. ISBN 978-0-470-63155-3.
- [26] MIKULASEK, T., GEORGIADIS, A., COLLADO, A., LACIK, J. 2x2 Microstrip Patch Antenna Array Fed by Substrate Integrated Waveguide for Radar Applications. *IEEE Antennas and Wireless Propagation Letters* [online]. 2013, **12**, 1287–1290. ISSN 1536-1225, 1548-5757. doi: 10.1109/LAWP.2013.2283731
- [27] IWASAKI, H. A circularly polarized small-size microstrip antenna with a cross slot - IEEE Journals & Magazine. *IEEE Transactions on Antennas and Propagation* [online]. 1996, **44**(10), 1399–1401. doi: 10.1109/8.537335

- [28] KIN-LU WONG, CHIEN-CHIN HUANG, WEN-SHAN CHEN. Printed ring slot antenna for circular polarization. *IEEE Transactions on Antennas and Propagation* [online]. 2002, **50**(1), 75–77. ISSN 1558-2221. doi: 10.1109/8.992564
- [29] CUPAL, M., DŘÍNOVSKÝ, J., GÖTTHANS, T., HERMÁNY, R., KOKOLIA, M., LÁČÍK, J., PAŘÍZEK, T., PRÁŠEK, J., RAIDA, Z., ŠPŮREK, J., KRÁČALOVÁ, D., LÉDROVÁ, Z., PROCHÁZKA, J., KRUTÍLEK, D., ŘEZNÍČEK, D. Textile-integrated electronics for small airplanes. In: *12th European Conference on Antennas and Propagation (EuCAP 2018)* [online]. 2018, p. 1–5. doi: 10.1049/cp.2018.0845
- [30] GHIOTTO, A., ADHIKARI, S., WU, K. Ferrite-Loaded Substrate Integrated Waveguide Switch. *IEEE Microwave and Wireless Components Letters* [online]. 2012, **22**(3), 120–122. ISSN 1531-1309. doi: 10.1109/LMWC.2012.2183859

CURRICULUM VITAE

Miroslav Cupal

Družstevní 890
572 01 Polička
Czech Republic

email: xcupal02@phd.feec.vutbr.cz
phone: +420 736 616 695

Education

2015 – current	Brno University of Technology, Brno, Czech Republic Ph.D., Electronics and Communication Research topic: Textile-integrated electronics
2013 – 2015	Brno University of Technology, Brno, Czech Republic MSc., Electronics and Communication Diploma thesis: In-car wireless power transfer
2010 – 2013	Brno University of Technology, Brno, Czech Republic BSc., Electronics and Communication Bachelor thesis: Implantable antennas for biomedical telemetry

Working experience and research stays

3/2012 to 8/2012	OMKO Digital, a.s. Service technician of satellite receivers
7/2014 to 8/2014	RETIA, .a.s. Technician of antenna systems
9/2014 to 12/2020	SIX Research Centre PhD researcher
01/2020 to present	Brno University of Technology
09/2020 to present	SINTEX, a.s. Designer of textile integrated electronics

Research projects

2017 to 2019	Interdisciplinary research of wireless technologies Ministry of Education, Youth and Sports, LO1401
2016 to 2017	Tools for the synthesis of antennas and sensors Technology Agency of the Czech Republic, TA04010457
10/2016 to present	Intelligent upholstery of vehicles (INTELUP) Ministry of Industry and Trade, FV10087

07/2019 to present Textile electronics for homecare and professional use (TED)
Ministry of Industry and Trade, FV40385

Language

English

Software skills

CST Microwave Studio,
MATLAB,
Python,
ANSYS Electromagnetic Desktop,
PSpice

ABSTRACT

The thesis is focused on the research of structures based on the Textile Integrated Waveguide (TIW). Attention is turned to the electrical characterization of textile materials (textile substrates, yarns) to be used for the implementation of textile-integrated antennas, reconfigurable and active circuits. The thesis deals with the design of multilayer transitions between a microstrip line on a conventional substrate and textile-integrated lines. Second, a concept of the textile-integrated switch is presented. The switch is controlled by conductive posts which are connected or disconnected by DC driven PIN diodes to form open or closed walls. Finally, the design methodology for textile-integrated circularly polarized antennas operating in ISM bands up to 24 GHz is proposed.

All the design procedures were verified by simulations and measurements of real samples manufactured by screen-printing using a silver polymer paste. For bonding semiconductor components, conductive silver adhesives were used. Screen-printed components were compared with reference structures manufactured from a self-adhesive copper foil.

ABSTRAKT

Práce je zaměřena na výzkum struktur založených na vlnovodu integrovaném do textilu (TIW). Pozornost je věnována elektrické charakterizaci textilních materiálů (textilní substráty, nitě), které jsou využívány při implementaci antén, rekonfigurovatelných a aktivních obvodů integrovaných do textilu. Práce se zabývá návrhem vícevrstvých přechodů mezi mikropáskovým vedením na konvenčním substrátu a vedeními integrovanými do textilu. Dále je prezentován koncept přepínače integrovaného do textilu. Přepínač je řízen vodivými sloupky, které vytvářejí otevřenou či zavřenou stěnu prostřednictvím stejnosměrně ovládaných PIN diod. Na závěr je formulována metodika návrhu kruhově polarizovaných antén integrovaných do textilu, jež jsou určeny pro práci v ISM pásmech až do 24 GHz.

Všechny postupy návrhu byly ověřeny simulacemi a měřeními reálných vzorků, které byly vyrobeny sítotiskem stříbrnou polymerovou pastou. Polovodičové komponenty byly k obvodům přilepeny vodivým stříbrným lepidlem. Komponenty vyrobené sítotiskem byly porovnávány s referenčními strukturami, které byly realizovány pomocí samolepicí měděné fólie.